Cavitation Influence on von Kármán Vortex Shedding and Induced Hydrofoil Vibrations

Philippe Ausoni

Mohamed Farhat

Laboratory for Hydraulic Machines,
EPFL, Ecole polytechnique fédérale de Lausanne,
Avenue de Cour 33bis,
1007 Lausanne, Switzerland

Xavier Escaler

Eduard Egusquiza

Center for Industrial Diagnostics,
UPC, Universitat Politecnica de Catalunya,
Avenidad Diagonal 647,
08028 Barcelona, Spain

François Avellan

Laboratory for Hydraulic Machines,
EPFL, Ecole polytechnique fédérale de Lausanne,
Avenue de Cour 33bis,
1007 Lausanne, Switzerland
e-mail: francois.avellan@epfl.ch

The present study deals with the shedding process of the von Kármán vortices at the trailing edge of a 2D hydrofoil at high Reynolds number $Re_h=25\times10^3$–65×10^3. This research focuses mainly on the effects of cavitation and fluid-structure interaction on the mechanism of the vortex generation. The vortex shedding frequency, derived from the flow-induced vibration measurement, is found to follow the Strouhal law provided that no hydrofoil resonance frequencies are excited, i.e., lock-off. For such a regime, the von Kármán vortices exhibit strong spanwise 3D instabilities and the cavitation inception index is linearly dependent on the square root of the Reynolds number. In the case of resonance, the vortex shedding frequency is locked onto the hydrofoil eigenfrequency and the spatial coherence is enhanced with a quasi-2D shape. The measurements of the hydrofoil wall velocity amplitude and phase reveal the first torsion eigenmotion. In this case, the cavitation inception index is found to be significantly increased compared to lock-off conditions. It makes clear that the vortex roll-up is amplified by the phase locked vibrations of the trailing edge. For the cavitation inception index, a new correlation relationship that encompasses the entire range of Reynolds numbers, including both the lock-off and the lock-in cases, is proposed and validated. In contrast to the earlier models, the new correlation takes into account the trailing edge displacement velocity. In addition, it is found that the transverse velocity of the trailing edge increases the vortex strength linearly. This effect is important in the context of the fluid-structure interaction, since it implies that the velocity of the hydrofoil trailing edge increases the fluctuating forces on the body. It is also demonstrated that cavitation developing in the vortex street cannot be considered as a passive agent for the turbulent wake flow. In fact, for fully developed cavitation, the vortex shedding frequency increases up to 15%, which is accompanied by the increase of the vortex advection velocity and reduction of the streamwise vortex spacing. In addition, a significant increase of the vortex-induced vibration level is found at cavitation onset. These effects are addressed and thought to be a result of the increase of the vorticity by cavitation. [DOI: 10.1115/1.2746907]

Introduction

Vortex shedding is the dominant feature of two-dimensional (2D) body wakes. Due to its fundamental importance and the wide range of industrial applications including heat exchangers, underwater drilling rig, and electric transmission lines, vortex shedding has been studied intensively for the flow past cylinders and some other bluff bodies. In contrast, the vortex shedding past hydrofoils has been studied to much less extent, particularly for high Reynolds numbers, despite numerous practical applications; for example, in ship propulsion and hydropower generation. The lack of experimental data for hydrofoils becomes particularly evident today, since engineers tend to use materials to their limits, causing structures to be more flexible, so that the vortex-induced vibrations become one of the primary damage mechanisms (Blevins [1]). For instance, it is found that the vibrations caused by von Kármán vortex shedding can cause premature and fatigue cracks in the stay vanes of turbines. Recently, Lockey et al. [2] and Shi [3] report on the damage of runners due to resonance regime, i.e., lock-in. Besides, depending on the pressure level in the flow, cavitation can occur in the shed vortices. However, except for several early studies, the phenomenon of cavitation developing in the shed vortices has been ignored for a long time. The goal of the present work is to investigate the effect of cavitation and fluid-structure interaction on the development of the von Kármán vortex street in the wake of a 2D hydrofoil at high Reynolds numbers. The role of the hydrofoil vibration in the cavitation inception and vortices strength is pointed out.

Placed in a fluid stream, bluff bodies generate separated flow over a substantial proportion of their surface that extends to their wake. The detachment of the boundary layers on both upper and lower surfaces forms two shear layers generating above critical values of Reynolds numbers, a periodic array of discrete vortices termed von Kármán street. In a range of upstream velocity, the vortex shedding frequency is known to follow the Strouhal law. From a hydrodynamic point of view, the instability of the shear layer separating from a circular cylinder has been extensively investigated; see Williamson and Roshko [4] for a comprehensive review. Many authors observe that the wake structure may exhibit a 3D aspect even if the obstacle and the upcoming flow are 2D. Gerrard [5] observed curved vortices and suspected that the cylinder end conditions might be the cause. Tritton [6] and Slaouti and Gerrard [7] report that vortices may be shed at a swept angle from the cylinder axis, which is called oblique shedding. Gerich and Eckelmann [8], Prasad and Williamson [9], and Williamson [10] find that the spanwise end conditions control the primary vortex shedding and significantly affect the stability of the separating shear layer.

Vortex-induced vibration and fluid-structure interaction phenomena have been subjected to much research, which Rockwell [11] and Williamson and Govardhan [12] have reviewed. It is well known that the bodies that shed spanwise vortices may be excited into oscillation by the fluctuating side forces resulting from such vortices. For instance, the resonance occurs when the vortex shed-

Contributed by the Fluids Engineering Division of ASME for publication in the JOURNAL OF FLUIDS ENGINEERING. Manuscript received June 27, 2006; final manuscript received March 16, 2007. Review conducted by Timothy J. O'Hern.

ding frequency coincides with one of the eigenfrequencies of the combined fluid-structure system. In the case where the response amplitude becomes sufficiently large, the structural displacement can control the fluid excitation, leading to the so-called "lock-in" phenomenon. The vortex shedding frequency is therefore "locked" onto the structural eigenfrequency over a rather extended range of free stream velocity magnitudes. With large structural displacement, the vortex strength is increasing as well as the periodic forces. And with the axial correlation of vorticity increasing, the periodic forces are further increased. Therefore, the vibration increases until the energy fed into the structure by the flow equals the energy dissipated per cycle. The response of freely vibrating cylinders is detailed by Feng [13]. For a lightly damped circular cylinder, vibration amplitude hysteresis is observed when reduced velocity is increased over a certain range and then is decreased back over the same range. However, this hysteresis is still to be fully explained. Davies [14] compared the wake structure for stationary and oscillating bluff bodies. The results showed an increase of 35% in the circulation of vortices shed from the oscillating cylinder, compared with those in the wake of a stationary body. Gilbert and Sigurdson [15] investigated the influence of the structural vibration on the vortex street morphology. They visualized hydrogen bubble flow of a self-oscillating cylinder vortex street "void." Interestingly, "voids" did not originate at nodes in the cylinder's vibration; they were seen to appear where the cylinder is vibrating at amplitudes that appear to be a large fraction of the cylinder's diameter.

When the pressure is low enough, bubbles filled with vapor and noncondensable gas are initiated and persist in the center of individual shed vortices. Sridhar and Katz [16] investigated the effect of entrained bubbles on the structure of vortex rings. They demonstrated that few microscopic bubbles are able to fragment the core of the vortex into two regions with peak vorticities that were 20% higher than the original maximum vorticity. Considering a Rankine vortex, Arndt and Keller [17] established that the maximum velocity in the cavitation vortex is $\sqrt{2}$ higher than in the noncavitating vortex. Young and Holl [18] investigated the case of a flow around wedges. They observed that the cavitation development in the wake increased the shedding frequency by up to 25% and therefore affected the dynamics of the von Kármán street. Dupont et al. [19] confirmed these results in the case of a 2D hydrofoil. Models for cavitation inception in the wake of bluff bodies have been presented by Belahadji et al. [20] and Arndt [21]. The models lead to a linear $\sigma_i \sim \sqrt{\mathrm{Re}_h}$ law that correctly predicts the correlation between the cavitation inception index and the Reynolds number for the considered range of upstream velocities. Although remarkably successful in describing the cavitation inception for fixed bluff bodies, none of these studies provides a direct insight into the role of the trailing edge vibration on the cavitation occurrence.

In this paper, the experimental setup and the measuring techniques are first presented. The following section is devoted to the experimental results of the fluid-structure interaction in the cavitation free regime: the vortex shedding frequency and the hydrofoil vibration amplitude are evidenced as well as the lock-in and the corresponding eigenmode. The next section studies the fluid-structure interactions' influence on cavitation inception: a direct insight is provided into the role of the hydrofoil trailing edge vibration. Finally, the cavitation development for both lock-off and lock-in conditions are illustrated through wake visualizations and flow-induced vibration analysis. The paper's conclusions are summarized in the last section.

Experimental Setup

The Ecole polytechnique fédérale de Lausanne (EPFL) high-speed cavitation tunnel, outlined in Fig. 1, is a closed loop with a test section of $150 \times 150 \times 750$ mm (Avellan et al. [22]). The operating flow parameters are the upstream velocity C_{ref} and the cavitation index σ. The incidence angle of the hydrofoil α is kept at 0 deg and the cavitation index is set above 0.2 to allow cavitation occurrence only in the wake and not on the hydrofoil wall.

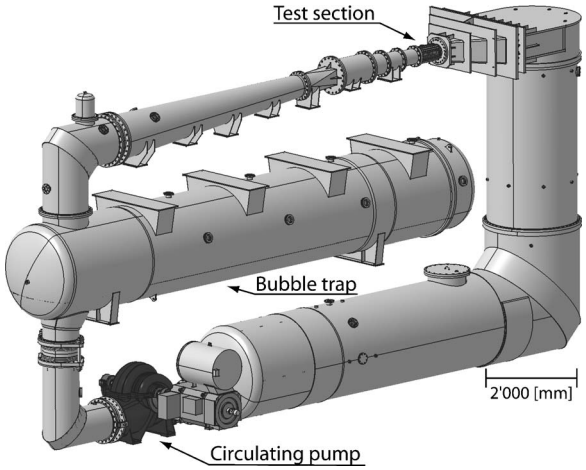

Fig. 1 EPFL high speed cavitation tunnel

The experimental 2D hydrofoil, sketched in Fig. 2, is a blunt truncated NACA 0009 made of stainless steel. The trailing edge thickness h is 3.22 mm and its chord length L and span b are 100 mm and 150 mm, respectively. The hydrofoil mounting in the test section can be considered as a perfect embedding on one side and pivot embedding on the other.

A specific optical probe is developed to investigate the vortex advection velocity, the shedding frequency and the intervortex spacing for different cavitation development. As sketched in Fig. 3, two parallel laser beams, 4 mm apart, which are periodically interrupted by the von Kármán vortex cavitation, are set to cross the wake. Two fast photodiodes are placed to track the light beam intensities modulated by the passing cavities. The probe is mounted on a traversing system, and measurements are performed at different locations in the wake.

The flow-induced vibrations are measured with the help of an accelerometer and a laser vibrometer. The piezoelectric accelerometer whose resonance frequency is 54 kHz is fitted on the profile support and a portable laser vibrometer is used to survey the hydrofoil wall vibrations. The measurement principle of the laser vibrometer is based on the detection of the frequency shift of the reflected laser beam according to the doppler effect; the frequency shift being directly related to the displacement velocity of the wall in the laser direction. The location of the vibration amplitude measurements points is shown in Fig. 4. Hydrofoil vibration measurements are synchronized with the accelerometer signal used as a reference. The amplitude and the phase of the hydrofoil motion for each measurement point are measured and the eigenmode is identified for the detected hydro-elastic coupling. The data acquisition system has 16 bits A/D resolution, 16 inputs, a memory depth of 1 MSamples per channel, and a maximum sampling frequency of 51.2 kHz per channel.

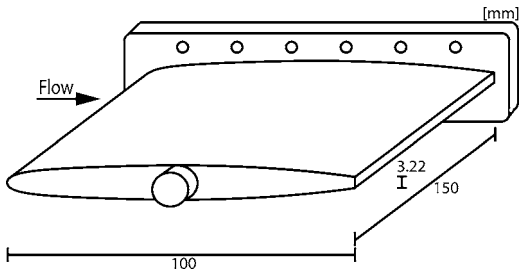

Fig. 2 Blunt truncated NACA 0009 hydrofoil

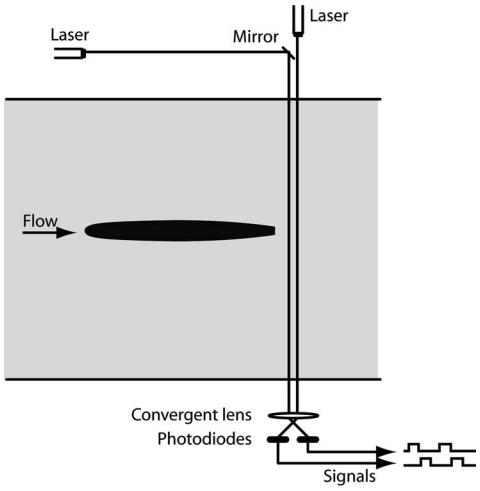

Fig. 3 Sketch of the double laser optical probe

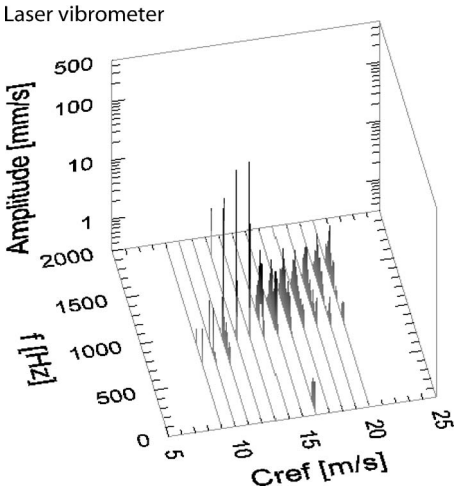

Fig. 5 Waterfall spectra of the laser vibrometer signals for different upstream velocities

The vortical structures in the wake are visualized with the help of a high speed digital camera. The CCD image resolution is 512×192 pixels at 10,000 frames/s, and the exposure time may be adjusted down to 10 μs.

Fluid-Structure Interactions in Cavitation Free Regime

The waterfall spectra of the laser vibrometer signals is presented in Fig. 5 for different upstream velocities. Most of the spectral energy is concentrated around a frequency that increases with the upstream velocity. We have identified this frequency as the shedding frequency of von Kármán vortices. The amplitude of the induced vibration changes according to the upstream velocity: as the vortex-shedding frequency approaches one of the natural frequencies of the combined fluid-structure system, the coupling takes place with a significant increase of noise and vibration levels. The vortex-shedding frequency is "locked" onto the structural eigenfrequency that is 900 Hz for flow velocity ranging from 11 m/s to 13 m/s; i.e., $\mathrm{Re}_h = 35{,}000$ to 42,000. In addition to the energy at the vortex-shedding frequency, all the spectra show energy for this eigenfrequency.

The vortex-shedding frequency normalized by the lock-in frequency and derived from the laser vibrometer and the accelerometer signals is presented in Fig. 6 as a function of the flow velocity. Both measuring techniques provide equivalent signal time history. A linear relationship between the vortex-shedding frequency and the upstream velocity is observed provided that no hydrofoil resonance frequencies are excited. For such a lock-off regime, the generation process of von Kármán vortices occurs at constant Strouhal number, i.e., St=0.24. The hydrofoil trailing edge vibration amplitude at the vortex shedding frequency is also evidenced in Fig. 6.

In lock-in conditions corresponding to 11–13 m/s upstream velocities, we observe the increase and decrease of the vibration amplitude. As the upstream velocity is increased and decreased, neither shedding frequency nor vibration amplitude reveal a hysteresis effect. For the above-mentioned lock-in condition, the hydrofoil wall vibration is surveyed by laser vibrometer measurements. As illustrated in Fig. 7, the modal shape is identified as the first torsion mode. The maximum vibration amplitude of the trailing edge is up to 0.2×10^{-3} m. For this condition, the vibration is found to be large enough to dominate the unsteady flow field and a self-controlled vibration is induced.

Fluid-Structure Interactions' Influence on Cavitation Inception

Bubbles are initiated in the individual vortices' centers, where the minimum pressure is reached. As previously described, models for cavitation inception in the wake of bluff bodies have already been proposed. The method is based on the known pressure distribution for either Rankine or Oseen models. Relating the vor-

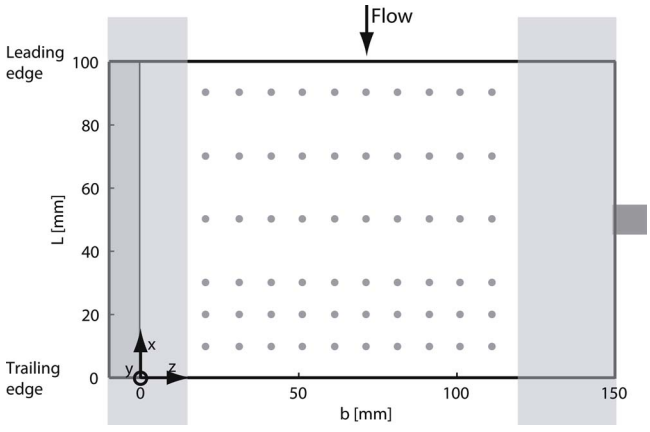

Fig. 4 Location of the hydrofoil vibration amplitude measurement points

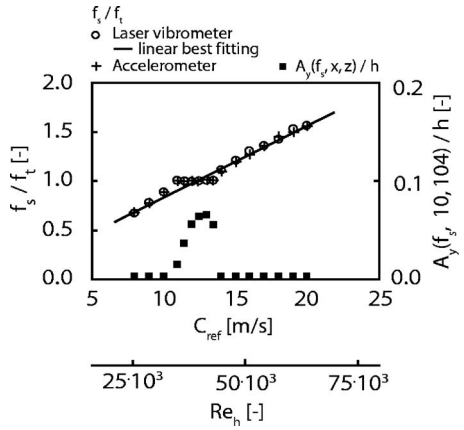

Fig. 6 Shedding frequency of von Kármán vortices and vibration amplitude of the hydrofoil trailing edge for different upstream velocities

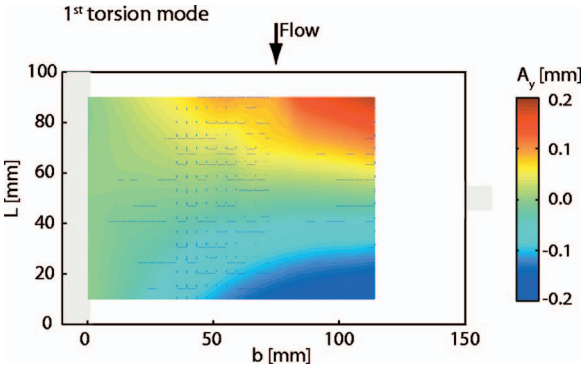

Fig. 7 Survey of the hydrofoil wall vibration amplitude for lock-in condition; C_{ref}=12 m/s

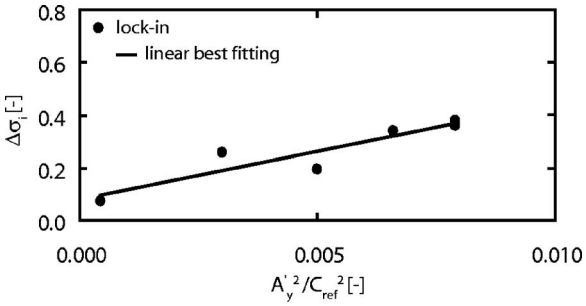

Fig. 9 Difference between the cavitation inception number in lock-in condition and the value derived from the linear regression of the cavitation inception numbers in lock-off condition versus the square of the hydrofoil trailing edge vibration velocity scaled by the upstream velocity

tex core diameter to the boundary-layer thickness, the method leads to a linear $\sigma_i \sim \sqrt{\mathrm{Re}_h}$ law, which correctly predicts the correlation between the cavitation inception index and the Reynolds number for the considered range of upstream velocities. Although successful in describing the cavitation inception for fixed bluff bodies, none of these studies provides a direct insight into the role of the trailing edge vibration on the cavitation occurrence. In the present study, the cavitation index inception values are presented in Fig. 8 as a function of the square root of the Reynolds number. Distinctions are made between lock-in and lock-off conditions.

For lock-off conditions, a linear tendency between the cavitation inception index and the square root of the Reynolds number is evidenced in Fig. 8 and is in accordance with former models. For lock-in conditions corresponding to the torsion mode, the cavitation inception index is significantly higher than for the lock-off conditions. The trailing edge vibration adds dynamic effects in the generation process of von Kármán vortices. The differences ($\Delta\sigma_i$) between the cavitation inception number in lock-in condition and the value derived from the linear regression of the cavitation inception numbers in lock-off condition is calculated and plotted in Fig. 9 as a function of the square of the hydrofoil trailing edge vibration velocity A'_y scaled by the upstream velocity C_{ref}. A clear linear relationship between $\Delta\sigma_i$ and $A'^2_y/C^2_{\mathrm{ref}}$ is achieved. The former models for wake cavitation inception have to be extended by taking into account the hydrofoil trailing edge displacement velocity as:

$$\sigma_i = a + b\sqrt{\mathrm{Re}} + c\frac{A'^2_y}{C^2_{\mathrm{ref}}} \tag{1}$$

Furthermore, if a cavitation free streamwise vortex is simply modeled as a Rankine vortex, the pressure p_c within the core of diameter a, is given by

$$p_{\mathrm{ref}} - p_c = \rho\left(\frac{\Gamma}{2\pi a}\right)^2 \tag{2}$$

At the cavitation inception in the vortex, the core pressure reaches the vapor pressure, i.e., $p_c = p_v$. According to the definition of the cavitation inception index, the relation (2) yields the following expression for the vortex strength Γ:

$$\frac{\Gamma}{a} = \pi C_{\mathrm{ref}}\sqrt{2\sigma_i} \tag{3}$$

By using the relation (3), the ratio Γ/a is evaluated for both lock-in and lock-off conditions. The observations of the vapor core size at cavitation inception for different upstream velocities under lock-in conditions and different vibration levels did not show any evidence of significant size changes. Therefore, it is believed that the influence of blade vibratory motion on the viscous core of the vortex is negligible and allows us to assume a constant core diameter. The differences $\Delta\Gamma$ between the calculated strength in lock-in condition and the value derived from the linear regression of the strength in lock-off condition Γ are then derived and plotted in Fig. 10 as a function of the trailing edge vibration velocity scaled by the upstream velocity A'_y/C_{ref}. In Fig. 10, a linear trend for the vortex strength increase in relation to the trailing edge vibratory velocity is observed. We have also presented the corresponding value found from the comparison of the wake structure for a stationary and oscillating cylinder [14] and this value matches remarkably well the linear relationship derived from our measurements. As mentioned by Davies [14], this increase in vortex strength is important in terms of fluid-structure interaction, since it implies that the hydrofoil trailing edge velocity increases the fluctuating forces on the body and this effect is additional to any increased spanwise coherent length, as observed for the resonance condition.

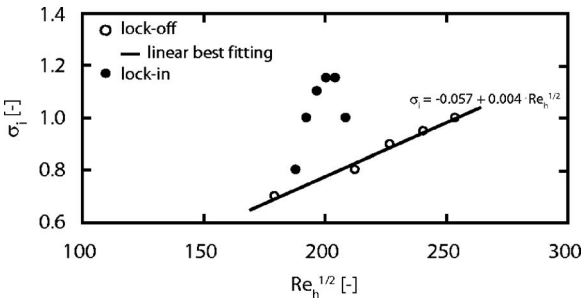

Fig. 8 von Kármán vortices cavitation inception index versus the square root of the Reynolds number

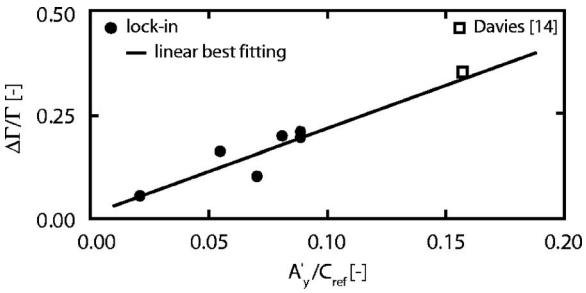

Fig. 10 Relative vortex strength for lock-in condition versus the hydrofoil vibration amplitude

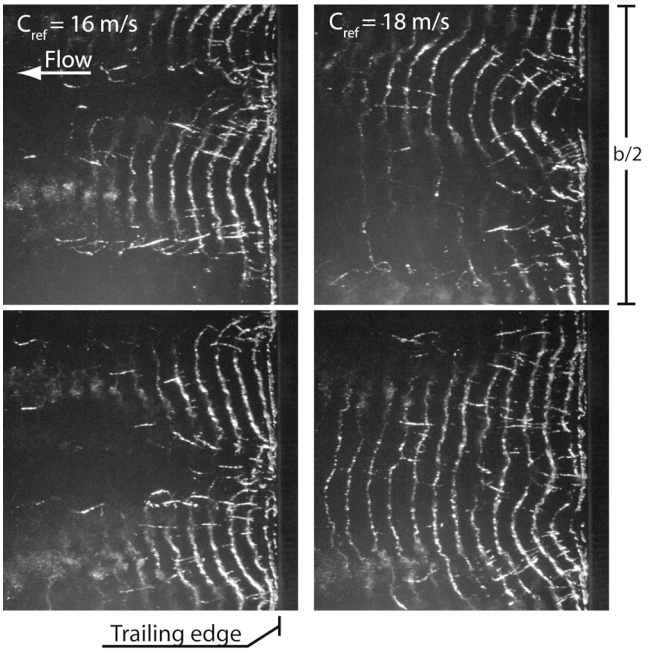

Fig. 11 Top-view photographs of von Kármán vortex street cavitation in lock-off conditions

Cavitation Development in Lock-Off Conditions

Two pairs of top-view photographs of cavitating vortex street in lock-off condition for two upstream velocities are presented in Fig. 11. It is observed that the wake exhibits 3D instabilities. The distortions and the spatial randomness of the vortical structures are evidenced. As already mentioned, the test section walls at both ends of the hydrofoil generate vorticity that can alter the 2D advection of the vortex street. The coherence length is, therefore, shorter as compared to the hydrofoil span.

For different values of cavitation index at 16 m/s upstream velocity, the waterfall spectra of the laser vibrometer signals is presented in Fig. 12, and shows notable influences of cavitation: as soon as the cavitation appears in the core of the von Kármán vortices ($\sigma/\sigma_i=1$), a significant increase of the shedding frequency but also of the structural vibration amplitude is observed. As the cavitation index is further reduced, the shedding frequency keeps increasing in an almost linear way and exceeds by 15% the cavitation free regime value. Although the shedding frequency increase with the development of the cavitation has already been observed in previous research for flow around wedges, the above-

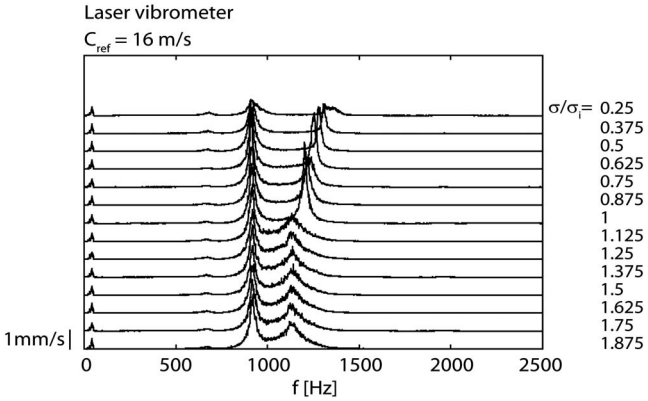

Fig. 12 Waterfall spectra of the laser vibrometer signals for different values of cavitation index and for lock-off condition

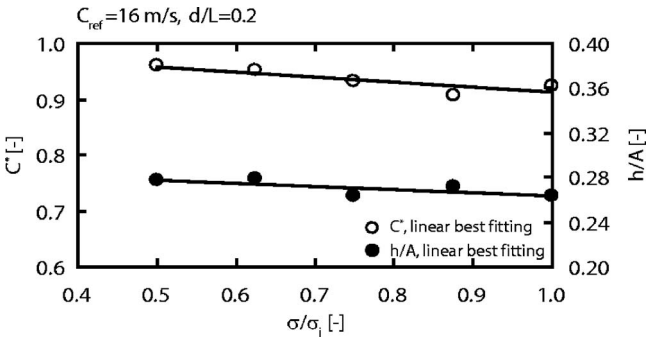

Fig. 13 Reduced advection velocity of the vortices and spacing ratio of the vortex street versus cavitation index for lock-off condition

mentioned increase of the vortex-induced vibration at early stage of cavitation has not been reported earlier. When the cavitation is fully developed ($\sigma/\sigma_i<0.4$), the vibration amplitude drops and the vortex structures merge to form a single vapor cavity at the trailing edge. Moreover, all the spectra show energy at 900 Hz corresponding to the eigenfrequency of the torsion mode.

The cavitation effects on the vortices' reduced advection velocity $C^*=C_{\text{Kármán}}/C_{\text{ref}}$ and the intervortex spacing h/A is presented in Fig. 13. The results correspond to a lock-off condition with an upstream velocity of 16 m/s. The distance from the trailing edge is 0.02 m, which is sufficiently far downstream from the vortex generation zone. It is observed that the vortices' advection velocity increases with the cavitation development as much as 4% for $\Delta\sigma=0.4$. This increase is linear and occurs as soon as the cavitation appears in the wake. By using the measurements of the vortices' advection velocity and their corresponding shedding frequencies, the intervortex spacing is evaluated by

$$A(t)=x(t+T)-x(t)=\int_t^{t+T} C_{\text{Kármán}}(\tau)d\tau \tag{4}$$

where $x(t)$ is the position of a vortex at time t and T is the vortex-shedding period. The ratio h/A is plotted for several cavitation index values in Fig. 13. Since the intervortex spacing is found to decrease for decreasing cavitation index, the ratio h/A increases with the development of the cavitation. h/A can be considered as an approximation of the spacing ratio B/A. In Fig. 13, for cavitation inception, the spacing ratio value reaches 0.27, which is close to the value 0.281 predicted by the von Kármán stability theory.

At the present stage, it becomes obvious that cavitation cannot be considered as a passive agent for the visualization of the turbulent wake flow. It is believed that the shedding frequency increase with the development of the cavitation can be explained by the interpretation of the description of the vortex street formation made by Gerrard [23]. The description postulates that a vortex continues to grow, fed by circulation from its connected shear layer, until it is strong enough to draw the opposing shear layer across the near wake. Sridhar and Katz [16] show that few microscopic bubbles fragment the core of the vortex into two regions with peak vorticities that are 20% higher than the original maximum vorticity. In the cavitating growing vortex, this higher vorticity draws sooner the opposing shear layer across the wake than in the cavitation free vortex. Consequently, the approach of oppositely signed vorticity cuts off sooner the supply of circulation to the growing vortex. The vortex shedding frequency is thus increased. Furthermore, the increase of the hydrofoil vibration at cavitation inception is likely attributed to the above-mentioned vorticity increase. In addition, as the vorticity increases and assuming a constant vortex core diameter, the maximum tangential velocity of the vortices and, therefore, their advection velocities increase. Considering a Rankine vortex, Arndt and Keller [17]

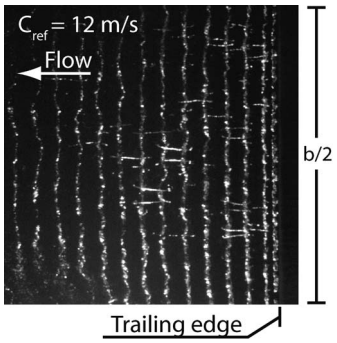

Fig. 14 Top-view photographs of cavitation von Kármán vortex street for lock-in condition (first torsion mode)

established that the maximum velocity in the cavitating vortex is $\sqrt{2}$ higher than in the noncavitating vortex and support our claim. As the vortex-shedding frequency and advection velocity increase, the intervortex spacing decreases for stability of the vortex street.

Cavitation Development in Lock-In Conditions

For lock-in, the trailing edge vibration leads to more organized wake structures. When the torsion mode is excited, the transverse motion of the trailing edge significantly increases the coherent length of the vortex street, and parallel vortex shedding takes place as evidenced in Fig. 14.

Frames of high speed visualizations of the von Kármán vortex street for lock-in condition are presented in Fig. 15 for moderated cavitation development (σ/σ_i=0.85), and full cavitation development (0.7). The five frames from top to bottom represent one generation cycle of a pair of von Kármán vortices. It can be observed that during the motion of the trailing edge from its minimum lower to its maximum upper transverse location, the volume

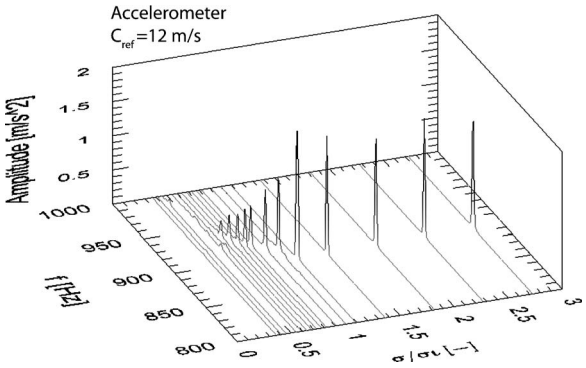

Fig. 16 Waterfall spectra of the acceleration signals for different values of cavitation index at 12 m/s upstream velocity

of vapor in the recirculation zone increases and starts rolling up without being advected by the mean flow. When the hydrofoil reaches its maximum displacement, the vortex detaches from the trailing edge and accelerates in the hydrofoil wake. As soon as the upper vortex has been detached, the lower one is generated in a similar way during the backward motion of the hydrofoil. Besides the primary von Kármán vortices, the wake also exhibits secondary vortices for the developed cavitation condition σ/σ_i=0.7. According to these visualizations, the roll-up of the separated shear layers takes place precisely at the rear face of the body. Therefore, we conceive that the displacement velocity of the trailing edge strongly acts on the generated vortices' strength, as previously evidenced.

As the vortex-shedding frequency tends to increase with the cavitation development, it is found possible to enable or disable hydro-elastic couplings just by permitting a sufficient cavitation development while keeping the upstream velocity constant. In Figs. 16 and 17, it is shown how the hydrofoil resonance is dis-

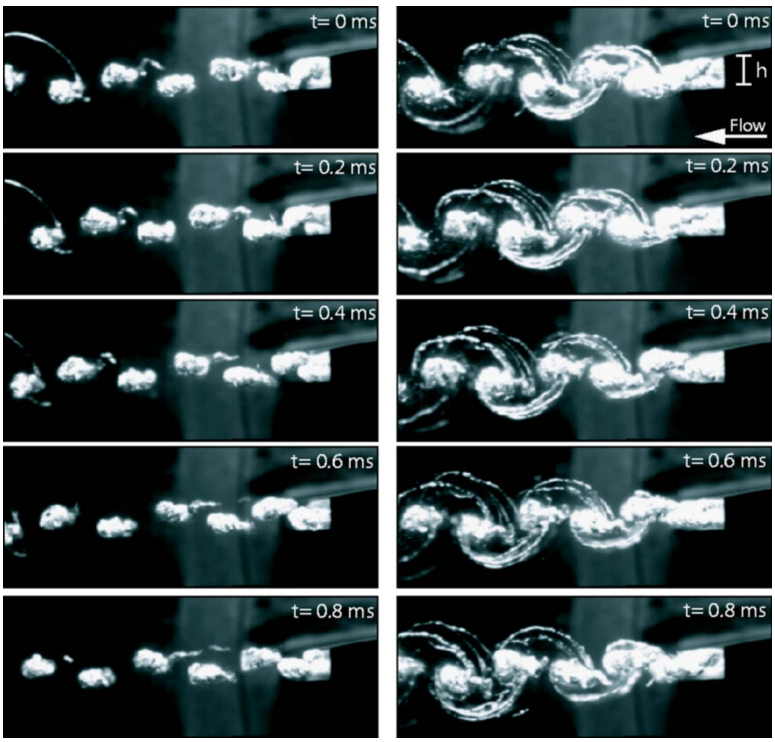

Fig. 15 Frame series of von Kármán vortex street for lock-in condition (first torsion mode; C_{ref}=12 m/s) and for two cavitation indices (left) σ/σ_i=0.85, (right) σ/σ_i=0.7

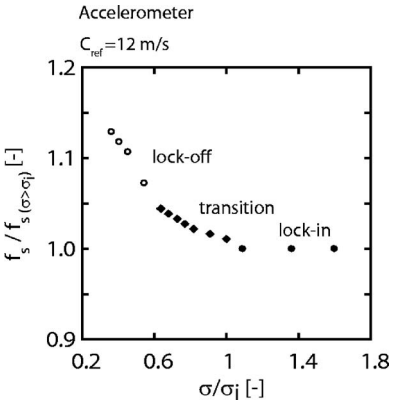

Fig. 17 Shedding frequency of von Kármán vortices versus cavitation index at 12 m/s upstream velocity

abled when the upstream velocity is maintained at 12 m/s, for which the torsion mode is excited in a cavitation free regime. In Fig. 16, waterfall spectra of the accelerometer signals for different values of cavitation index are presented. Figure 17 illustrates the vortex shedding frequency f_s, normalized by its corresponding value for the cavitation free regime $f_s(\sigma > \sigma_i)$ versus the cavitation index. As the cavitation appears in the wake and develops, the vortex-shedding frequency increases, but at a lower rate than in the case out of resonance. Although the amplitude of vibration decreases, the resonance is maintained since the amplitudes remain higher than in the lock-off condition. The structural vibration therefore tends to control the unsteady flow field and forces the vortices to be shed near the eigenfrequency. Upon further decrease of the cavitation index, the coupling is no longer maintained, so that the vortex-shedding frequency increases in a more marked way.

Conclusions

The von Kármán vortex street generated in the wake of a 2D hydrofoil with a truncated trailing edge is investigated in the EPFL high speed cavitation tunnel. The data are obtained for a wide range of cavitation indices and Reynolds numbers; i.e., $\mathrm{Re}_h = 25 \times 10^3 - 65 \times 10^3$. Combination of high speed visualization, laser optical probe, and measurements of flow-induced vibration provides a unique way of analyzing the dynamics of the von Kármán vortex street. The mutual effects of hydrofoil vibration and cavitation development on the mechanism of the vortex generation are pointed out.

In cavitation free regime, the shedding frequency of von Kármán vortices occurs at a constant Strouhal number provided that no hydrofoil resonance frequencies are excited; i.e., lock-off. In the case of resonance (lock-in), the vortex-shedding frequency is locked onto the hydrofoil eigenfrequency and the vortex coherent length is significantly increased. The measurements of the hydrofoil wall velocity amplitude and phase reveal the first torsion eigenmotion.

It is demonstrated that cavitation developing in the vortex street cannot be considered as a passive agent for the turbulent wake flow. In fact, for fully developed cavitation, the vortex-shedding frequency increases up to 15%, accompanied by the increase of the vortex advection velocity and reduction of the streamwise vortex spacing. In addition, a significant increase of the vortex-induced vibration level is found at cavitation onset, which has never before been reported. These effects are addressed and are thought to be a result of the increase of the vorticity by cavitation.

The wake cavitation inception index is linearly dependent on the square root of the Reynolds number in the lock-off regime, which agrees well with the earlier experimental observations. However, in the lock-in regime, the cavitation inception index is significantly higher than in the lock-off case, and it is no longer linearly dependent on the Reynolds number. For the cavitation inception index, a new correlation relationship that encompasses the entire range of Reynolds numbers, including both the lock-off and the lock-in cases, is proposed and validated. In contrast to the earlier models, the new correlation takes into account the trailing edge displacement velocity. In addition, it is found that the transverse velocity of the trailing edge increases the vortex strength linearly. This effect is important in the context of the fluid-structure interaction, since it implies that the velocity of the hydrofoil trailing edge increases the fluctuating forces on the body.

Acknowledgment

The investigation reported in this paper is part of the work carried out for the HYDRODYNA, Eureka Research Project No. 3246, whose partners are ALSTOM Hydro, EDF-CIH, EPFL, GE Hydro, UPC-CDIF, VATECH Hydro, and VOITH-SIEMENS Hydro Power Generation. The project is also financially supported by CTI, the Swiss Federal Commission for Technology and Innovation Grant No. 7045-1 and NSF, the Swiss National Science Foundation Grant No. 2000-068320. The authors are very grateful to the HYDRODYNA Technical Committee for its involvement and constant support to the project. Finally the staff of the EPFL Laboratory for Hydraulic Machines should be thanked for its support in the experimental and numerical work.

Nomenclature

A = vortex row spacing, m
$A_y(f_s,x,z)$ = hydrofoil vibration amplitude for the shedding frequency f_s at coordinates (x,z), m
A'_y = hydrofoil vibration velocity, m/s
b = hydrofoil span, m
B = distance between vortex rows, m
C_{ref} = reference velocity at the test section inlet, m/s
$C_{\mathrm{Kármán}}$ = vortex advection velocity, m/s
C^* = reduced advection velocity, $C^* = C_{\mathrm{Kármán}}/C_{\mathrm{ref}}$
f_s = vortex shedding frequency, Hz
f_t = hydrofoil torsion eigenfrequency, Hz
L = hydrofoil chord length, m
p_{inlet} = reference pressure at the test section inlet, bar
p_v = vapor pressure, bar
Re_h = Reynolds number, $\mathrm{Re}_h = C_{\mathrm{ref}} h/\nu$
St = Strouhal number, $\mathrm{St} = f_s h/C_{\mathrm{ref}}$
h = hydrofoil trailing edge thickness, m
α = incidence angle of the hydrofoil, deg
σ = cavitation index, $\sigma = 2(p_{\mathrm{inlet}} - p_v)/\rho C_{\mathrm{ref}}^2$
σ_i = cavitation inception index
ν = kinematic viscosity, m^2/s

References

[1] Blevins, R. D., 1985, "The Effect of Sound on Vortex Shedding From Cylinders," J. Fluid Mech., **161**, pp. 217–237.
[2] Lockey, K. J., Keller, M., Sick, M., Staehle, M. H., and Gehrer, A., 2006, "Flow-Induced Vibrations at Stay Vanes: Experience on Site and CFD Simulations," Int. J. Hydropow. Dams, **5**, pp. 102–106.
[3] Shi, Q., 2004, "Abnormal Noise and Runner Cracks Caused by von Karman Vortex Shedding: A Case Study in Dachaoshan Hydroelectric Project, Proceedings of the 22nd IAHR Symposium on Hydraulic Machinery and Systems," Stockholm, Sweden, Paper No. A13-2:1–12.
[4] Williamson, C. H. K, and Roshko, A., 1998, "Vortex Formation in the Wake of an Oscillating Cylinder," J. Fluids Struct., **2**, pp. 355–381.
[5] Gerrard, J. H., 1978, "Wakes of Cylindrical Bluff Bodies at Low Reynolds-Number," Philos. Trans. R. Soc. London, Ser. A, **288**(1354), pp. 351–382.
[6] Tritton, D. J., 1959, "Experiments on the Flow Past a Circular Cylinder at Low Reynolds Number," J. Fluid Mech., **6**, pp. 547–567.
[7] Slaouti, A., and Gerrard, J. H., 1981, "An Experimental Investigation of the End Effects on the Wake of a Circular Cylinder Towed Through Water at Low Reynolds Number," J. Fluid Mech., **112**, pp. 297–314.
[8] Gerich, D., and Eckelmann, H., 1982, "Influence of End Plates and Free Ends on the Shedding Frequency of Circular Cylinders," J. Fluid Mech., **122**, pp. 109–122.

[9] Prasad, A., and Williamson, C. H. K., 1997, "The Instability of the Shear Layer Separating From a Bluff Body," J. Fluid Mech., **333**, pp. 375–402.
[10] Williamson, C. H. K., 1988, "Defining a Universal and Continuous Strouhal-Reynolds Number Relationship for the Laminar Vortex Shedding of a Circular Cylinder," Phys. Fluids, **31**, pp. 2742–2744.
[11] Rockwell, D., 1998, "Vortex-Body Interactions," Annu. Rev. Fluid Mech., **30**, pp. 199–229.
[12] Williamson, C. H. K., and Govardhan, R., 2004, "Vortex-Induced Vibrations," Annu. Rev. Fluid Mech., **36**, pp. 413–455.
[13] Feng, C. C., 1968, "The Measurement of Vortex-Induced Effects in Flow Past Stationary and Oscillating Circular and D-Section Cylinders," MS thesis, Univ. Br. Columbia, Vancouver, Canada.
[14] Davies, M. E., 1975, "A Comparison of the Wake Structure of a Stationary and Oscillating Bluff Body, Using a Conditional Averaging Technique," J. Fluid Mech., **75**, pp. 209–231.
[15] Gilbert, S, and Sigurdson, L., 2005, "Hydrogen Bubble Flow Visualization of a Self-Oscillating Cylinder Vortex Street 'Void'," Phys. Fluids, **17** p. 091104.
[16] Sridhar, G., and Katz, J., 1999, "Effect of Entrained Bubbles on the Structure of Vortex Rings," J. Fluid Mech., **397**, pp. 171–202.
[17] Arndt, R. E. A., and Keller, A. P., 1992, "Water Quality Effects on Cavitation Inception in a Trailing Vortex," J. Fluids Eng., **114**, pp. 430–438.
[18] Young, J., and Holl, J., 1966, "Effects of Cavitation on Periodic Wakes Behind Symmetric Wedges," J. Basic Eng., **88**, pp. 163–176.
[19] Dupont, P., Avellan, F., and Wegner, M., 1987, "Wake Flow Analysis for a Hydrofoil With and Without Hydroelastic Lock-In," Proc. Int. Conf. on Flow Induced Vibrations, BHRA, Bowness-on-Windermere, England.
[20] Belahadji, B., Franc, J. P., and Michel, J. M., 1995, "Cavitation in the Rotational Structures of a Turbulent Wake," J. Fluid Mech., **287**, pp. 383–403.
[21] Arndt, R. E. A., 1976, "Semi-Empirical Analysis of Cavitation in the Wake of a Sharp-Edged Disk," ASME J. Fluids Eng., **90**, pp. 560–562.
[22] Avellan, F., Henry, P., and Ryhming, I. L., 1987, "A New High Speed Cavitation Tunnel," ASME Winter Annual Meeting, Boston, MA, Vol. 57, pp. 49–60.
[23] Gerrard, J. H., 1966, "The Mechanics of the Formation Region of Vortices Behind Bluff Bodies," J. Fluid Mech., **25**, pp. 401–413.